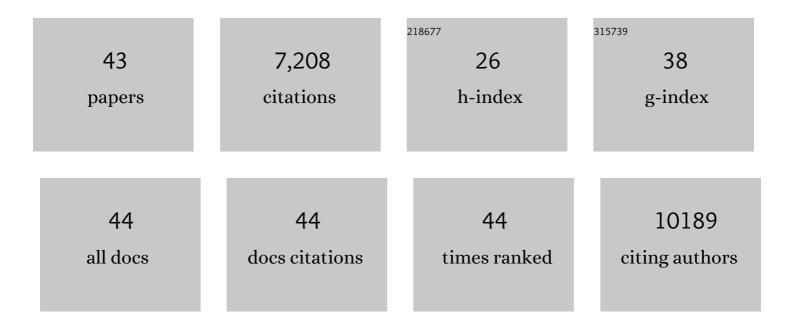
Michael E Oskin

List of Publications by Year in descending order

Source: https://exaly.com/author-pdf/5569255/publications.pdf Version: 2024-02-01



#	Article	IF	CITATIONS
1	Near-Field High-Resolution Maps of the Ridgecrest Earthquakes from Aerial Imagery. Seismological Research Letters, 2022, 93, 494-499.	1.9	9
2	Accrual of widespread rock damage from the 2019 Ridgecrest earthquakes. Nature Geoscience, 2022, 15, 222-226.	12.9	23
3	Late Pleistocene slip rate of the central Haiyuan fault constrained from optically stimulated luminescence, 14C, and cosmogenic isotope dating and high-resolution topography. Bulletin of the Geological Society of America, 2021, 133, 1347-1369.	3.3	18
4	Documentation of Surface Fault Rupture and Ground-Deformation Features Produced by the 4 and 5 July 2019 MwÂ6.4 and MwÂ7.1 Ridgecrest Earthquake Sequence. Seismological Research Letters, 2020, 91, 2942-2959.	1.9	47
5	An analysis of the factors that control fault zone architecture and the importance of fault orientation relative to regional stress. Bulletin of the Geological Society of America, 2020, 132, 2084-2104.	3.3	14
6	Characteristic slip distribution and earthquake recurrence along the eastern Altyn Tagh fault revealed by high-resolution topographic data. , 2020, 16, 392-406.		16
7	Segmented Thrust Faulting: Example From the Northeastern Margin of the Tibetan Plateau. Journal of Geophysical Research: Solid Earth, 2020, 125, e2019JB018634.	3.4	11
8	Airborne Lidar and Electro-Optical Imagery along Surface Ruptures of the 2019 Ridgecrest Earthquake Sequence, Southern California. Seismological Research Letters, 2020, 91, 2096-2107.	1.9	31
9	Reevaluation of the Late Pleistocene Slip Rate of the Haiyuan Fault Near Songshan, Gansu Province, China. Journal of Geophysical Research: Solid Earth, 2019, 124, 5217-5240.	3.4	35
10	Extent of Lowâ€Angle Normal Slip in the 2010 El Mayorâ€Cucapah (Mexico) Earthquake From Differential Lidar. Journal of Geophysical Research: Solid Earth, 2019, 124, 943-956.	3.4	9
11	Paleoseismic Investigation of the Aksay Restraining Double Bend, Altyn Tagh Fault, and Its Implication for Barrierâ€Breaching Ruptures. Journal of Geophysical Research: Solid Earth, 2018, 123, 4307-4330.	3.4	20
12	Geomorphic offsets along the creeping Laohu Shan section of the Haiyuan fault, northern Tibetan Plateau. , 2018, 14, 1165-1186.		30
13	A 6000-year-long paleoseismologic record of earthquakes along the Xorkoli section of the Altyn Tagh fault, China. Earth and Planetary Science Letters, 2018, 497, 193-203.	4.4	34
14	Surface Slip From the 2014 South Napa Earthquake Measured With Structure From Motion and 3â€Đ Virtual Reality. Geophysical Research Letters, 2018, 45, 5985-5991.	4.0	9
15	Structure and geometry of the Aksay restraining double bend along the Altyn Tagh Fault, northern Tibet, imaged using magnetotelluric method. Geophysical Research Letters, 2017, 44, 4090-4097.	4.0	34
16	Steady ¹⁰ Beâ€derived paleoerosion rates across the Plioâ€Pleistocene climate transition, Fish Creekâ€Vallecito basin, California. Journal of Geophysical Research F: Earth Surface, 2017, 122, 1653-1677.	2.8	8
17	Pulsed exhumation of interior eastern Tibet: Implications for relief generation mechanisms and the origin of high-elevation planation surfaces. Earth and Planetary Science Letters, 2016, 449, 176-185.	4.4	100
18	The role of a keystone fault in triggering the complex El Mayor–Cucapah earthquake rupture. Nature Geoscience. 2016. 9. 303-307.	12.9	60

MICHAEL E OSKIN

#	Article	IF	CITATIONS
19	Surfaceâ€Rupture and Slip Observations on the Day of the 24 August 2014 South Napa Earthquake. Seismological Research Letters, 2015, 86, 1119-1127.	1.9	12
20	Eastern termination of the Altyn Tagh Fault, western China: Constraints from a magnetotelluric survey. Journal of Geophysical Research: Solid Earth, 2015, 120, 2838-2858.	3.4	32
21	Geologic and structural controls on rupture zone fabric: A field-based study of the 2010 Mw 7.2 El Mayor-Cucapah earthquake surface rupture. , 2015, 11, 899-920.		52
22	Rupture termination at restraining bends: The last great earthquake on the Altyn Tagh Fault. Geophysical Research Letters, 2015, 42, 2164-2170.	4.0	63
23	Coseismic fault zone deformation revealed with differential lidar: Examples from Japanese <mml:math xmlns:mml="http://www.w3.org/1998/Math/MathML" altimg="si1.gif" overflow="scroll"><mml:msub><mml:mrow><mml:mi mathvariant="normal">M</mml:mi </mml:mrow><mml:mrow><mml:mrow><mml:mi></mml:mi></mml:mrow></mml:mrow></mml:msub></mml:math 	4.4 → <td>83 ath>â^1⁄47</td>	83 ath>â^1⁄47
24	Intraplate earthquakes. Earth and Planetary Science Letters, 2014, 405, 244-236. Relationship of channel steepness to channel incision rate from a tilted and progressively exposed unconformity surface. Journal of Geophysical Research F: Earth Surface, 2014, 119, 366-384.	2.8	7
25	Assembly of a large earthquake from a complex fault system: Surface rupture kinematics of the 4 April 2010 El Mayor–Cucapah (Mexico) Mw 7.2 earthquake. , 2014, 10, 797-827.		127
26	Optimization of legacy lidar data sets for measuring nearâ€field earthquake displacements. Geophysical Research Letters, 2014, 41, 3494-3501.	4.0	47
27	Coseismic slip variation assessed from terrestrial lidar scans of the El Mayor–Cucapah surface rupture. Earth and Planetary Science Letters, 2013, 366, 151-162.	4.4	60
28	Point-based computing on scanned terrain with LidarViewer. , 2013, 9, 546-556.		12
29	Thick deltaic sedimentation and detachment faulting delay the onset of continental rupture in the Northern Gulf of California: Analysis of seismic reflection profiles. Tectonics, 2013, 32, 1294-1311.	2.8	41
30	Stable, rapid rate of slip since inception of the San Jacinto fault, California. Geophysical Research Letters, 2013, 40, 4209-4213.	4.0	29
31	Near-Field Deformation from the El Mayor–Cucapah Earthquake Revealed by Differential LIDAR. Science, 2012, 335, 702-705.	12.6	206
32	Inherited strikeâ€slip faults as an origin for basementâ€cored uplifts: Example of the Kungey and Zailiskey ranges, northern Tian Shan. Tectonics, 2012, 31, .	2.8	61
33	Focused modern denudation of the Longmen Shan margin, eastern Tibetan Plateau. Geochemistry, Geophysics, Geosystems, 2011, 12, n/a-n/a.	2.5	51
34	Topographic control of asynchronous glacial advances: A case study from Annapurna, Nepal. Geophysical Research Letters, 2011, 38, n/a-n/a.	4.0	38
35	Deformation processes adjacent to active faults: Examples from eastern California. Journal of Geophysical Research, 2010, 115, .	3.3	60
36	Late Quaternary slip rate gradient defined using highâ€resolution topography and ¹⁰ Be dating of offset landforms on the southern San Jacinto Fault zone, California. Journal of Geophysical Research, 2010, 115, .	3.3	56

MICHAEL E OSKIN

#	Article	IF	CITATIONS
37	Palinspastic restoration of NAVDat and implications for the origin of magmatism in southwestern North America. Journal of Geophysical Research, 2010, 115, .	3.3	37
38	Southern California Earthquake Center Geologic Vertical Motion Database. Geochemistry, Geophysics, Geosystems, 2008, 9, .	2.5	8
39	The Shuttle Radar Topography Mission. Reviews of Geophysics, 2007, 45, .	23.0	5,113
40	Transient landscape evolution of basement ored uplifts: Example of the Kyrgyz Range, Tian Shan. Journal of Geophysical Research, 2007, 112, .	3.3	40
41	Exhumation of basement-cored uplifts: Example of the Kyrgyz Range quantified with apatite fission track thermochronology. Tectonics, 2006, 25, n/a-n/a.	2.8	129
42	Alpine landscape evolution dominated by cirque retreat. Geology, 2005, 33, 933.	4.4	94
43	Effects of bedrock landslides on cosmogenically determined erosion rates. Earth and Planetary Science Letters, 2005, 237, 480-498.	4.4	242